Assessing rainfall threshold for shallow landslides triggering: a case study in the Alpes Maritimes region, France

Sophie Barthelemy, Séverine Bernardie, Gilles Grandjean

Natural Hazards
https://doi.org/10.1007/s11069-024-06941-2

ORIGINAL PAPER

Assessing rainfall threshold for shallow landslides triggering: a case study in the Alpes Maritimes region, France

Sophie Barthélemy[1,2] · **Séverine Bernardie**[1] · **Gilles Grandjean**[1]

Received: 2 November 2023 / Accepted: 1 October 2024

Abstract

In this work, we use a statistical approach for modeling shallow landslide rainfall thresholds (Caine 1980) with a case study for the Alpes-Maritimes region (France). Cumulated rainfall / duration (ED) thresholds are obtained with the CTRL-T algorithm (Melillo and al. 2018) for different non-exceedance probabilities from a landslide and two climatic datasets. This tool allows to automatically define rainfall events that might trigger landslides, ensuring robustness and objectivity in this process. The first climate dataset stores high resolution gridded rainfall data (1km resolution, hourly), which provides rainfall data with high temporal and spatial accuracy. This dataset, coming from radar data, is calibrated with rainfall gauges, ensuring a higher accuracy of the rainfall measurements. It provides the rainfall records directly used in the threshold construction The second dataset contains lower resolution gridded rainfall, snow, temperature, and evapotranspiration data (8km resolution, daily); it enables to assess the region's climate through parameters imported in CTRL-T. The thresholds are then validated using a method designed by Gariano and et al. (2015). Several improvements are made to the initial method. First, evapotranspiration values approximated in the process are replaced by values from the second climate dataset, the result accounting best for the regional climate. Then, computing duration values used for isolating events and sub-events for each mesh point allows to consider the heterogeneity of the Alpes-Maritimes climate. Rainfall thresholds are eventually obtained, successively from a set of probable conditions (MRC) and a set of highly probable conditions (MPRC). The validation process strengthens the analysis as well as enables to identify best performing thresholds. This work represents novel scientific progress towards landslide reliable warning systems by (a) making a case study of empirical rainfall thresholds for Alpes-Maritimes, (b) using high-resolution rainfall data and (c) adapting the method to climatically heterogeneous zones.

Keywords Shallow landslides · Rainfall thresholds · French Alpes-Maritimes · CTRL-T · Gridded rainfall data

✉ Séverine Bernardie
s.bernardie@brgm.fr

Sophie Barthélemy
s.barthelemy@brgm.fr

[1] Present Address: BRGM, 3 avenue claude Guillemin, PB 36009, 45060 Orléans Cedex 02, France

[2] CNRM, Université de Toulouse, Météo-France, CNRS, Toulouse, France

1 Introduction

In many regions in the world, the principal trigger of shallow landslides is rainfall, causing fatalities, isolating population, and resulting in damage and economic losses. Forecasting the occurrence of landslides is one of the ways of mitigating the risk and of protecting the population. In that purpose, rainfall thresholds constitute a widely used tool to predict the possible occurrence of a landslide, especially applied at a territorial scale (Guzzetti et al. 2008). Different approaches can be founded for defining thresholds (Guzzetti et al. 2007): empirically, statistically (based on past conditions that resulted in landslides) or using physically-based (related to physical concepts such as slope stability models). The physically-based approach can be used for susceptibility models, dynamically (considering water table level) or in combination with threshold models. These methods are very interesting but have still some limitations. Indeed, in most of study, the studied area is small, at local scale. This is due to different elements needed for this kind of models; indeed physically-based models over large areas require big computational needs (Alvioli and Baum 2016). Moreover, geological, geotechnical and hydrogeological information at high resolution is necessary to feed these models, while these data are usually available only for small areas. At the contrary, statistical approaches are very interesting at territorial scale, as they require less computer means and less accurate input data.

A rainfall threshold for landslide triggering can be defined as a set of rainfall, soil moisture or hydrological conditions that, when reached or exceeded, are prone to initiating landslides. The first rainfall threshold proposed in the literature (Caine 1980) is a curve of equation $I = \alpha D^{-\beta}$ separating triggering and non-triggering intensity (I) /duration (D) conditions. Empirical thresholds are most often based on rainfall events characteristics, that can be intensity/duration (ID), cumulated rainfall (E)/ duration (D) / (ED) or intensity/cumulated rainfall (IE). Depending on studies, intensity parameter can be defined considering peak intensity or mean intensity. The cumulated rainfall E is defined as the sum of precipitations within an event, and the difference of their definition depends on the extents of the rainfall events. For instance, Peruccacci et al. (2012) defined a rainfall event that is preceded and followed by a dry period of a certain period, depending on the season. Some models take into account the antecedent rainfall as well (Guzzetti et al. 2007). The scope of this work being to define a single threshold for a whole territorial unit (French department) in the perspective of a future LEWS, we made the choice to work with empirical thresholds.

A lot of publications can be found using statistical rainfall thresholds (Aleotti 2004; Guzzetti et al. 2007; Brunetti et al. 2010; Segoni et al. 2014; Melillo et al. 2018). Moreover, Segoni et al. (2018) recently performed a review of 107 papers on rainfall thresholds for landslide triggering, analyzing different features such as: rain gauge selection, type of threshold, threshold parameters, validation method, and landslide type. The most used characteristics of rainfall are the intensity, cumulated rainfall, and duration of the rainfall event.

A high variety exists in the objectives, uses and characteristics of rainfall thresholds (Segoni et al. 2018). This review highlights the necessity of using an automatic procedure for all steps for defining thresholds, as it ensures robustness and objectivity. Moreover, the quality of input data (rainfall data and landslide database) is of great importance for obtaining a reliable threshold, even more as the final objective is to design a Landslide Early Warning System (LEWS). Most studies dedicated to landslide rainfall threshold determination are based on rain gauge data. However, the use of this data has

some limits (Marra et al. 2014), as: i) the rain gauge network often has a low density, with heterogeneous locations, ii) the spatial distribution might lack representativeness, especially in high altitude mountains where few rain gauges are installed. These limits lead to a systematic underestimation of the triggering conditions. At the contrary, remote–sensing observations, and among them weather radar rainfall, provide a high temporal and spatial resolution rainfall estimation (Marra et al. 2014). However, radar rainfall estimates are to be carefully considered, as several factors (i.e., meteorological, instrumental) might decrease its accuracy. Several procedures can be applied for correcting the bias, including a correction based on rain gauge data.

Finally, a critical key point revealed by Segoni et al. (2018), is related to the lack of validation of the method. The rainfall threshold validation, associated to the performance of LEWS constitutes a key step into the effectiveness of the system. Several authors propose some methodologies; most of them exploit a contingency table (Wilks 2006). Piciullo et al. (2020) have listed the indicators used by authors (Tiranti and Rabuffetti 2010; Staley et al. 2013; Segoni et al. 2015) for validating rainfall thresholds. These indicators are based on the four elements of the contingency table: true positive TP, true negative TN, false positive FP, false negative FN. These methods are interesting, as they provide objectivity and standardization (Segoni et al. 2018).

Recently, an algorithm was developed by Melillo et al. (2018), which enables to design thresholds considering input rainfall and landslide data. The algorithm also performs the intermediate steps of reconstructing significant rainfall events, made of sub-events, (Melillo et al. 2015) and selecting rain gauges. Both events and sub-events are generated by extracting from the rainfall record rainy periods isolated by dry periods superior to a given duration. The dry period required is smaller for sub-events than for events, and changes with the time of the year. Indeed, as evapotranspiration is higher in the dry season, smaller periods are considered to reset the influence of rainfall on soils. Results are very satisfying, and CTRL-T is used in several studies (Melillo et al. 2018; Teja et al. 2019; Gariano et al. 2019, 2020; Jordanova et al. 2020; Abraham et al. 2021). Based on this code, the methodology or input data might be improved, such as the assessment of some climatic parameters (e.g., evapotranspiration ratio).

In this paper, we present an alternative methodology for estimating landslide rainfall thresholds, using the algorithm CTRL-T, tailored to the Alpes Maritime department (France), the first step towards an operational LEWS. The advances rest in the use of high-resolution radar-derived rainfall data, a local assessment of the climate parameters, and the validation of the obtained thresholds.

In a first section, the study site is described, and we present the methodology that has been applied, providing the main features of the software and the improved characterization of the climatic parameters. Guidelines from Segoni et al. (2018) will be cautiously applied to rise above limitations of existing works. This methodology analyses the contingency table, the receiver operating characteristic (ROC) and the related skill scores. The various datasets used in this study are also described, from landslide inventory to rainfall and climate data. The results are then presented in another section, in the light of similar works completed in Europe. The validation step, based on the method proposed by Gariano et al. (2015), is then described and commented. Finally, the results are discussed, pointing out the significant outcomes and the limits of the approach that might be improved.

2 Methods

2.1 Threshold definition

Even though ID thresholds are most commonly found in the literature, we decided to use ED thresholds as event duration and event cumulated rainfall are independent variables, and consequently establishing a relationship is more statistically appropriate (Peruccacci et al. 2012).

The methodology used in this work is the one developed within the CTRL-T algorithm (Melillo et al. 2018). This choice is based on one principal aspect: it entirely automates the threshold creation process, only taking as input a landslide inventory, rainfall records and additional, region-specific climate parameters. The code CTRL-T is split in three functional blocks: a first block builds rainfall events using the continuous rainfall records and the climate parameters, a second block associates the landslide occurrences to the rainfall events to establish triggering conditions, and the last block operates on this pool of conditions to assess thresholds. The flowchart of CTRL-T is displayed on Fig. 1.

The concept of the first block is to define rainfall events and sub-events for each individual record (i.e., from rain gauges or gridded data). The raw rainfall records and the rain gauge locations are imported as well as a set of climate-dependent parameters, that are detailed in Melillo et al. 2018. The study describing CTRL-T (Melillo et al. 2018), makes use of a method based on the Monthly Soil Water Balance (MSWB) model (Thornthwaite and Mather 1957) for evaluating for the entire study zone the start (sws) and end (ews) of the warm season, and the ratio R of the cold and warm seasons' durations. The different steps necessary for obtaining these parameters are described in Melillo et al. 2018).

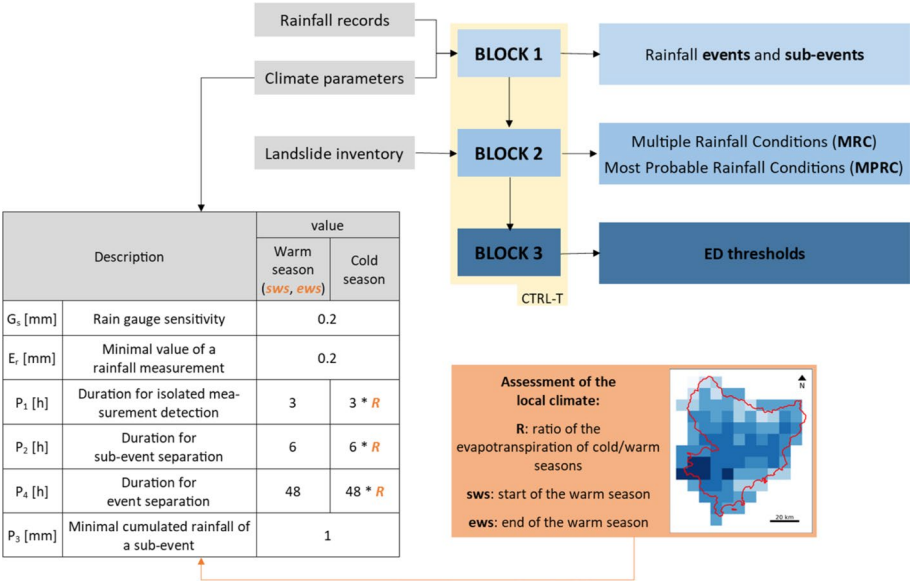

Description		value	
		Warm season (*sws*, *ews*)	Cold season
G_s [mm]	Rain gauge sensitivity	0.2	
E_r [mm]	Minimal value of a rainfall measurement	0.2	
P_1 [h]	Duration for isolated measurement detection	3	3 * *R*
P_2 [h]	Duration for sub-event separation	6	6 * *R*
P_4 [h]	Duration for event separation	48	48 * *R*
P_3 [mm]	Minimal cumulated rainfall of a sub-event	1	

Fig. 1 Flowchart of the CTRL-T algorithm with focus on the climate parameters

Amongst these steps, mean monthly values of potential evapotranspiration ($\overline{PET_m}$) are approximated from mean monthly values of temperature and the latitude of the study area. The subsequent steps consist in estimating real evapotranpiration from this potential evapotranspiration, and from this determine an aridity index, whose monthly values eventually indicate the extent of warm and cold seasons, useful for computing the R ratio.

An improvement of this approach is proposed in this study, by replacing the approximated MSWB $\overline{PET_m}$ by modeled PET values included in our second rainfall dataset, with a lower resolution. Moreover, considering single values of sws, ews and R for the whole study zone is not adapted to the Alpes-Maritimes area as its climate is heterogenous (Fig. 2). To fix this issue a second improvement is suggested: sws, ews and R are computed separately for each mesh point (equivalent to a station). This allowed obtaining a varying range of durations for a single region. To assess the importance of these climate-dependent parameters, we included in the analysis a comparison to rainfall thresholds obtained with a fixed R (R = 1 and R = 4, with a warm season starting in May and ending in September).

The second block of CTRL-T confronts the newly created rainfall events and sub-events to the landslide records. For each landslide occurrence, sub-events of the last rainfall event of geographically close rain gauges are combined to generate conditions. Two pools of conditions are created: Multiple Rainfall Conditions (MRC), which include all conditions from a single rain gauge for each landslide, and Most Probable Rainfall Conditions (MPRC) restraining the number of conditions per landslide to one. The selection of MPRC from MRC is based on a weight coefficient favoring intense events featuring high cumulated

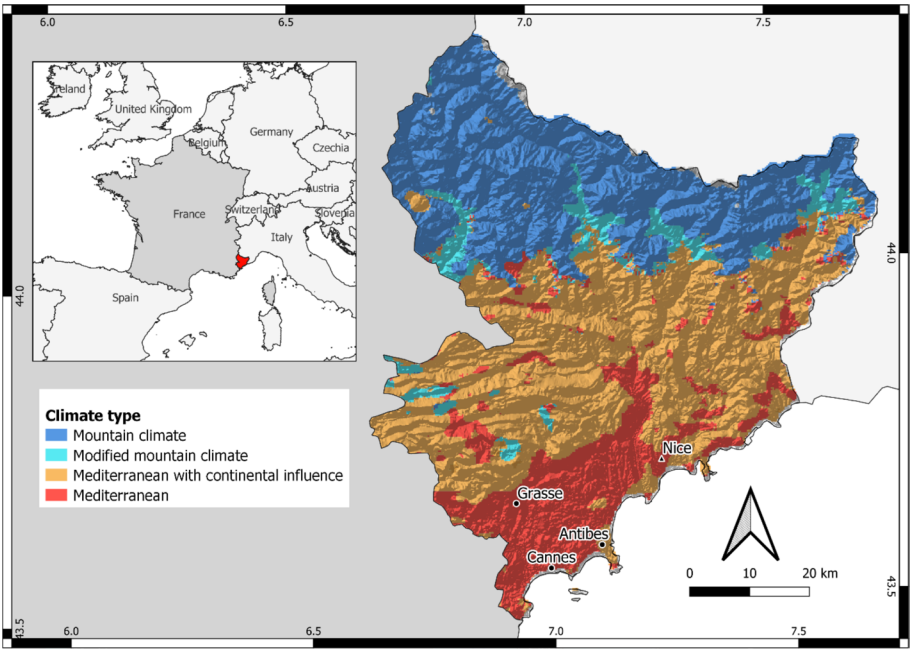

Fig. 2 Simplified climate map of Alpes-Maritimes department (based on (Joly et al. 2010). Mountain climates are represented in the north and Mediterranean climates in the south along the Mediterranean coastline. Cities featuring a population above 50.000 are as well indicated. Nice, the Prefecture of Alpes-Maritimes is specified with a triangle

rainfall recorded in stations geographically close to the landslide event. We consider that rainfall separated by more than 48 h to a landslide occurrence cannot have triggered the movement. Therefore, landslide events isolated from rainfall conditions in such manner are discarded from the analysis.

Finally, the third block generates rainfall thresholds for different non-exceedance probabilities (NEPs) using successively the MRC and the MPRC pools of triggering conditions. The definition of the thresholds is based on a frequentist approach (Brunetti et al. 2010) coupled to a bootstrap for uncertainty assessment (Peruccacci et al. 2012). This method enables obtaining a linear equation from a single (D, E) dataset and a given non-exceedance probability. A bootstrap completes this technique: the process is repeated with k randomly sampled series of m (D, E) couples from the same dataset. k linear coefficients are obtained from these series of m couples. The mean and standard deviation of these coefficients respectively represent the final coefficient value and the uncertainty. The process is repeated for a series of non-exceedance probabilities, first for the MRC then for the MPRC datasets. The obtained thresholds have a power law equation of the type $E = (\alpha \pm \Delta\alpha)D^{(\gamma \pm \Delta\gamma)}$.

In this work, we set the bootstrap parameters to k = 100 and m varying from 10 to the population size, similarly to what was done by (Melillo et al. 2018), which allowed us to assess the variations of uncertainty with the number of landslides. We repeated the process setting the non-exceedance probability parameter to 16 possible values: 50%, 35%, 20%, 10%, 9%, 8%, 7%, 6%, 5%, 4%, 3%, 2%, 1.5%, 1%, 0.5% and 0.005%.

2.2 Validation

In a second phase, a validation process has been carried out on the MPRC thresholds. The methodology (Gariano et al. 2015), requiring an independent dataset, has been designed specifically for ED thresholds obtained with a frequentist approach coupled to a bootstrap.

A pre-processing of the sub-events, following the method developed by (Gariano et al. 2015), is done. It consists of several steps. First, the sub-events of the validation set are compared to the validation MPRC. We identify the sub-events that form the MPRC as triggering (red markers). To avoid repetition, all sub-events recorded at the same time than the triggering condition by neighboring rain gauges are discarded (yellow markers). Then, rainfall sub-events whose durations were not included in the threshold validity range are removed (grey markers). The remaining sub-events are considered non-triggering (blue markers).

Then the predictive performance of the thresholds is estimated by counting contingencies (True Positives, True Negatives, False Positives and False Negatives), and then by computing skill scores: Probability of Detection (POD), Probability of False Detection (POFD), Probability of False Alarms (POFA), and Hanssen-Kuipers (HK) Skill Score. The POD quantifies the sensitivity of a system, i.e., the ability to predict true positives. The POFD is on the other hand equal to 1 minus the specificity of the system, which is the ability to predict true negatives. The POFA describes the proportion of false alarms in relation to the number of positives. Ultimately, the HK skill score is equal to the subtraction of POD and POFD.

We then determined which NEP led to the best performing threshold by performing a ROC Analysis (Fawcett 2006), method designed to assess the performance of binary classifiers.

The three blocks of CTRL-T are available in http://geomorphology.irpi.cnr.it/tools/rainfall-events-and-landslides-thresholds/ctrl-algorithm/ctrl-code/CTRL_code.R/; Melillo et al. 2018). The preparation of the datasets, the validation steps and the analysis were carried out with Python scripts.

3 Study area and data

3.1 Study area

The analysis has been carried out in the French Alpes-Maritimes department, located in South-East of France. Alpes-Maritimes department (4200 km^2) shares a border with Italy and faces the Mediterranean Sea. The north sector of the territory intersects the Alps Mountain range.

The Alpes-Maritimes department has experienced numerous episodes of intense rainfall over the last twenty years, with some particularly notable in terms of intensity, such as in 2000, in February and November 2014, October 2015, generating damaging landslides (see ORRM 2023).

The climate of the south of Alpes-Maritimes is Mediterranean, i.e., characterized by dry and hot summers. On the opposite, the climate of the northern zone of this territory is a mountain climate, in which the summers are warm to cool, and where no dry season is observed. The location as well as the climate zoning of Alpes-Maritimes is represented on Fig. 2, according to the climate classification defined by (Joly et al. 2010). Some other climate classification can be found and are described, such as the Köppen classification (Kottek et al. 2006; Rubel et al. 2017). Thus the studied area integrates the Csa, Csb, Cfb, Dfb and ET climates. This climate diversity needs to be considered as the methodology and process for defining rainfall threshold take into account the local climate. The rainfall data from the different climate areas will consequently receive a different processing.

This analysis is confirmed by precipitation (sum of rainfall and snowfall) statistics computed on the Safran dataset (described a few sections below) presented in Fig. 3. A and B display the average year cumulated precipitation, mapped and as time series. On the other hand, C and D respectively map the average cumulated precipitation of the driest and wettest months in the year. We indeed can subdivide the region in three zones: an area in the North more subjected to rainfall, a drier area in the South and a transition zone between the two of them. The amount of cumulated precipitation in a year averaged over the entire zone varies between 600 and 1300 mm. This indicator does not present any apparent time evolution pattern.

In the Southern, Mediterranean-climate area of the department, the average cumulated rainfall of the driest month between 1959–2016 ranges between 4 and 8 mm, whereas it is two to three times more important in the North, mountain climate area. This pattern is also observed for the average year and wettest month cumulated rainfall.

3.2 Landslide data

The landslide inventory, provided by the French Geological Survey (BRGM), is based on BRGM-CEREMA (https://www.georisques.gouv.fr/donnees/bases-de-donnees/base-de-donnees-mouvements-de-terrain) and RTM (https://bdrtm.onf.fr) databases, Department 06 Council, Regional Major Hazards Observatory (ORRM) and some municipalities

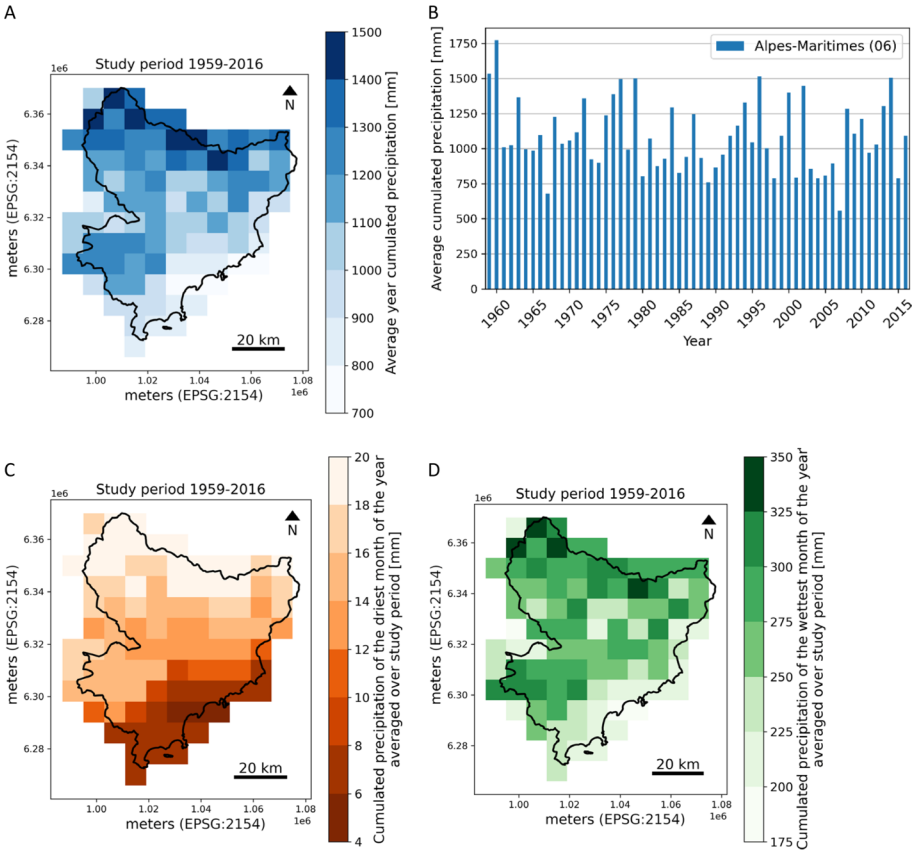

Fig. 3 Assessment of the climate of Alpes-Maritimes (from the Safran rainfall dataset presented below). Precipitation is obtained summing rainfall and snow variables. Mean year cumulated precipitation mapped over the area (**A**); spatial mean of cumulated precipitations per year (**B**). Average cumulated precipitation of the driest and wettest months in a year, respectively in (**C**) and (**D**)

data, and completed within the Interreg ALCOTRA AD-VITAM program (https://www.interreg-alcotra.eu/fr/ad-vitam), consists of 941 events that occurred in Alpes-Maritimes between 1905 and 2015. All landslides in the database are shallow landslides, with volumes estimated between a few m^3 to a maximal volume around 20 000 m^3. From this information, we selected events whose occurrence dates were precisely known (known day of occurrence) and that occurred in the time window for which rainfall data was available (1997–2016). 597 events were discarded, which left 344 events fitted to the analysis. This initial dataset is then split in two subsets: a calibration dataset, from which thresholds are generated, and an independent validation dataset designed to assess the thresholds. The calibration set compiles 269 landslides (78.2%) that occurred between 1997 and 2013, and the validation set is made of 75 landslides (21.8%) that occurred between 2014 and 2015. We willingly subdivided the initial dataset in two continuous periods: the aim was to preserve year rainfall patterns, in a warning-system perspective.

The yearly, monthly distributions, and a map of the landslides of both sets are featured on Fig. 4. The number of landslides is not constant over the years: the years 2000 and 2014 account for more than half of the documented events. Figure 4C indicates that most of the landslides of 2000 occurred in November and October, and in November and January for 2014. These time windows are correlated with exceptionally intense rainfall events documented by Météo-France (Météo-France 2023), including storms Rebekka and Qendresa. The graph displaying the monthly distributions of landslides underlines that most of the events occur during cold seasons: November and January accumulate the highest numbers. The spatial distribution of landslides, depicted on the map, also brings out relevant information. Even though mountain relief is highly favorable to the occurrence of landslides, most of them have been observed along the coastline, nearby urban zones. A bias exists in our landslide inventory as this denotes that most certainly much more landslides occurred in the mountain yet have not been documented.

3.3 Rainfall data

Two rainfall datasets, provided by Météo-France, were used in the present study. The first dataset, named Comephore, contains high-resolution rainfall data. It consists of hourly rainfall values issued from a reanalysis (Tabary et al. 2012) starting from the 01/01/1997 to the 31/12/2016, in each point of a 1 km-meshed grid covering Alpes-Maritimes department. This quantitative precipitation estimation, with high spatial and temporal accuracy, covers this area with no spatial nor temporal gaps. It is based on radar data providing pseudo-CAPPI reflectivity images that have been pre-processed and converted into rainfall rates. A radar/rain gauge calibration factor field has then been computed, and applied to the daily radar accumulation. In the case no calibration factor can be obtained, due to a lack of rain gauge, the daily radar accumulation is given by ordinary kriging of daily precision rain gauges. For computational purposes, we only considered the values of the 30 days before each landslide occurrence to compute the thresholds, taking Comephore mesh points located less than 1 km away from these same landslides. The time filtering was not applied over the validation period, the entirety of the rainfall data being relevant for this step. The selection of Comephore mesh points and landslide locations are plotted on Fig. 5.

The second dataset, named Safran, provides additional variables, with a lower resolution. Safran (*Système d'analyse fournissant des renseignements atmosphériques à la neige*) (Durand et al. 1993), initially developed for snow modeling, generates from observations and interpolates on a grid a set of atmospheric forcing (among which rain and snowfall). Assets of using the Safran dataset include the robustness of the analysis over long time periods (Vidal et al. 2010), and its good correlation with field observations (Quintana-Seguí et al. 2008). In our version of the dataset, rainfall, snow, temperature, and evapotranspiration values are available over France on an 8 km meshed grid with a daily time step from 01/08/1958 onwards. The SAFRAN dataset proved itself useful as the climate analysis developed by (Melillo et al. 2018) requires both precipitation and temperature fields, Comephore lacking the latter. The nearest Safran points to the Comephore selection (Fig. 5) are used to compute sws, ews and R parameters for the 1995–2015 period.

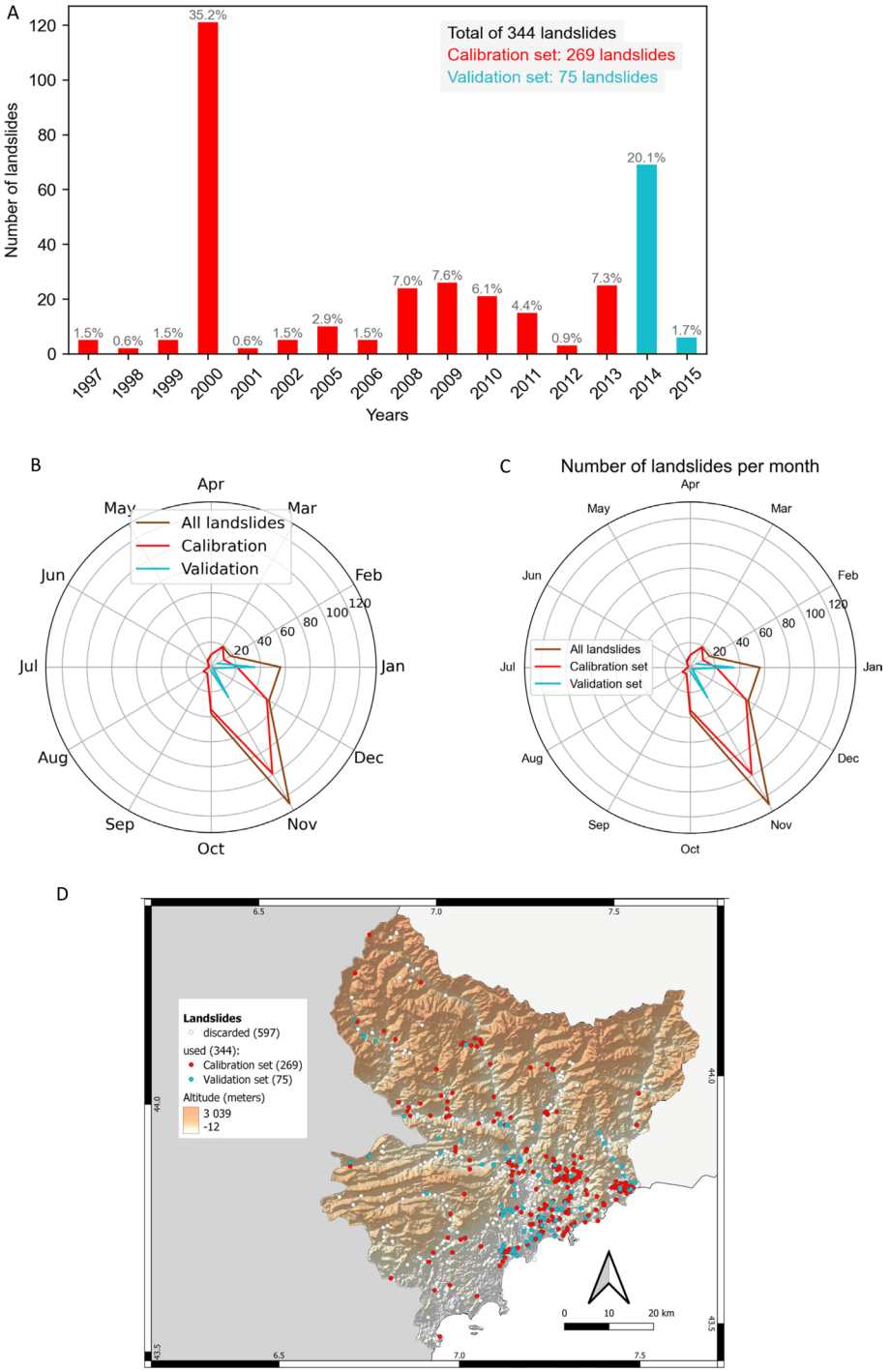

Fig. 4 Yearly (**A**) and monthly (**B**) distributions of the calibration and validation landslide datasets. The monthly distributions of the years 2000 and 2014 are available in a separate plot (**C**). Relief map of Alpes-Maritimes featuring landslides from the calibration and validation datasets, and discarded landslides (**D**)

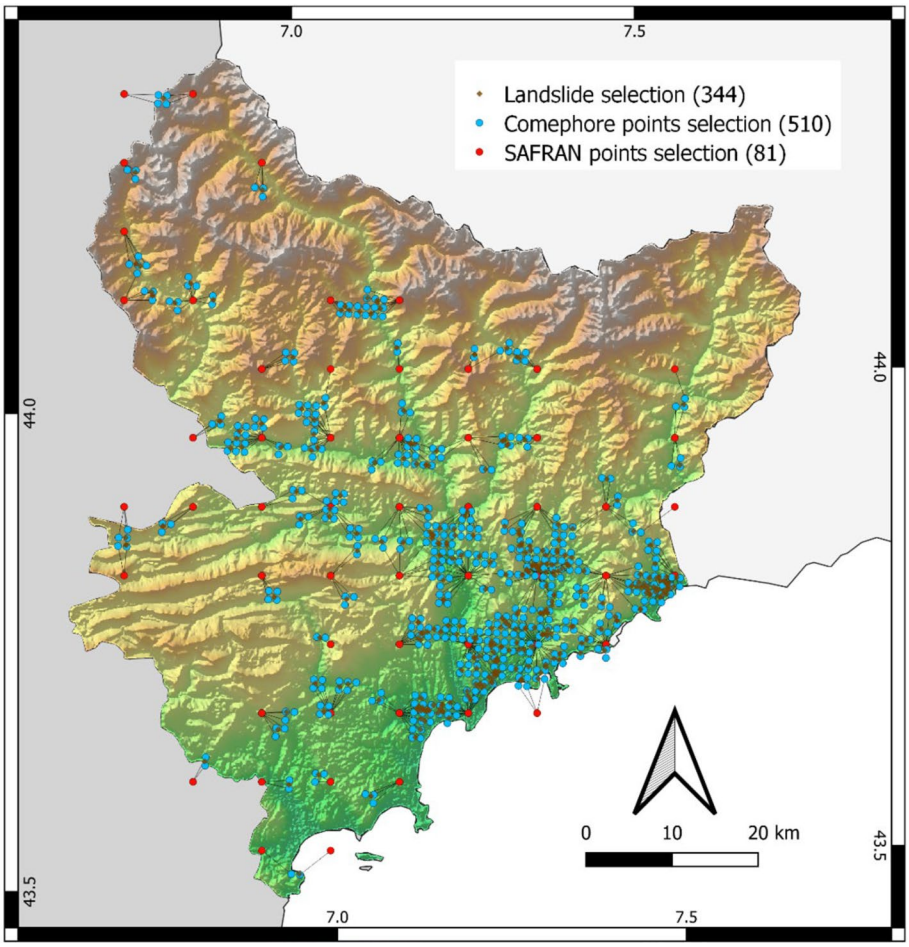

Fig. 5 Selected Comephore and Safran stations along with the landslide dataset. Comephore points (blue) have first been selected based on their geographical proximity to landslides (brown), and then Safran stations (red) were associated to Comephore

4 Results

4.1 Climate analysis

The parameters obtained from the climate analysis on the selection of Safran mesh points is on Fig. 6.

The start of the warm season varies from February (2) to June (6), and the end from August (8) to September (9). On the other hand, the value of the R ratio ranges from 1 to 4, depending on the SAFRAN mesh points.

To illustrate the difference, the results of the climate analysis for a mountain station and a Mediterranean station are represented in Fig. 7.

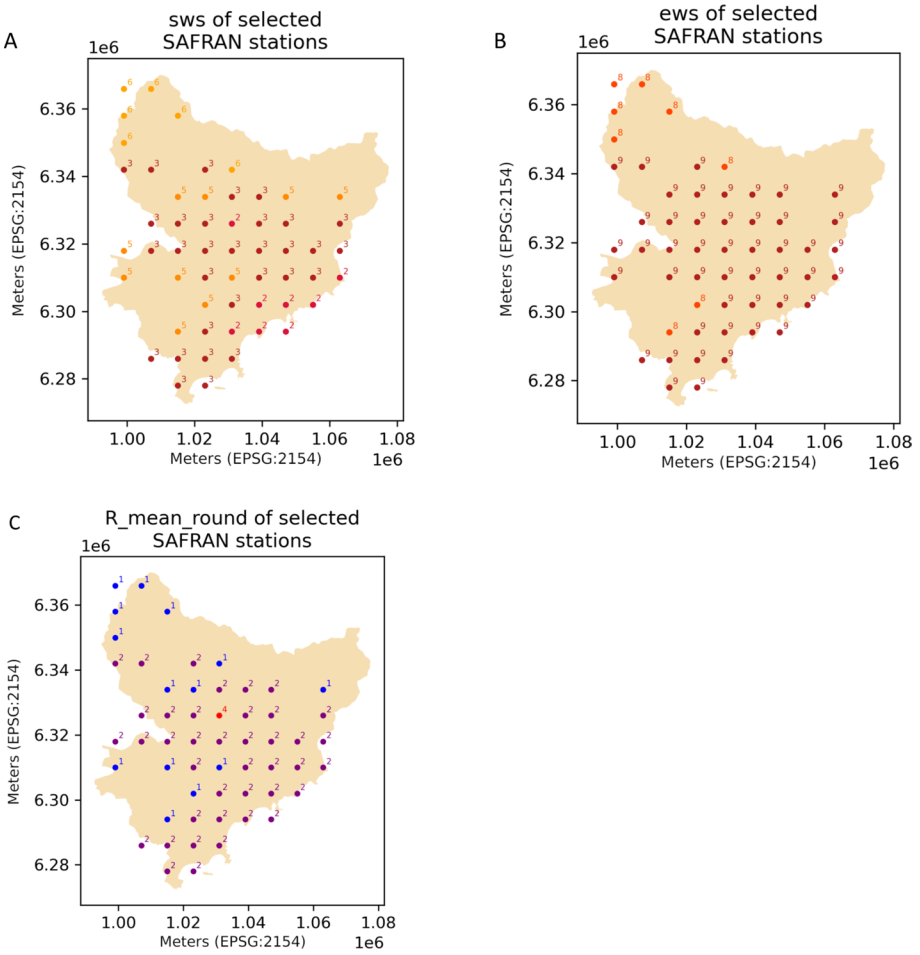

Fig. 6 Results of the climate analysis made on the nearest SAFRAN points to the Comephore points, over the period 1995–2015. Are represented month numbers respectively marking the start of the warm season (**A**), the end of the warm season (**B**) and the rounded ratio of the cold and warm seasons durations' (**C**)

4.2 Thresholds

Several rainfall thresholds are obtained from the calibration set, for different non-exceedance probabilities. 51 landslide events, separated from rainfall by more than 48 h, were discarded out of the initial 269 events chosen for the calibration, leaving 218 landslides for which conditions are reconstructed. The characteristics (equation, number of conditions, validity range and relative uncertainty) of the thresholds obtained from the calibration set are available in Table 1.

We also computed thresholds from this set considering constant climate-dependent parameters over the whole region (R = 1 and R = 4, with the warm season starting in May and ending in September). The equations and characteristics of the obtained 5% NEP thresholds are as well included in Table 1. All the NEP can be seen in Supplementary materials section.

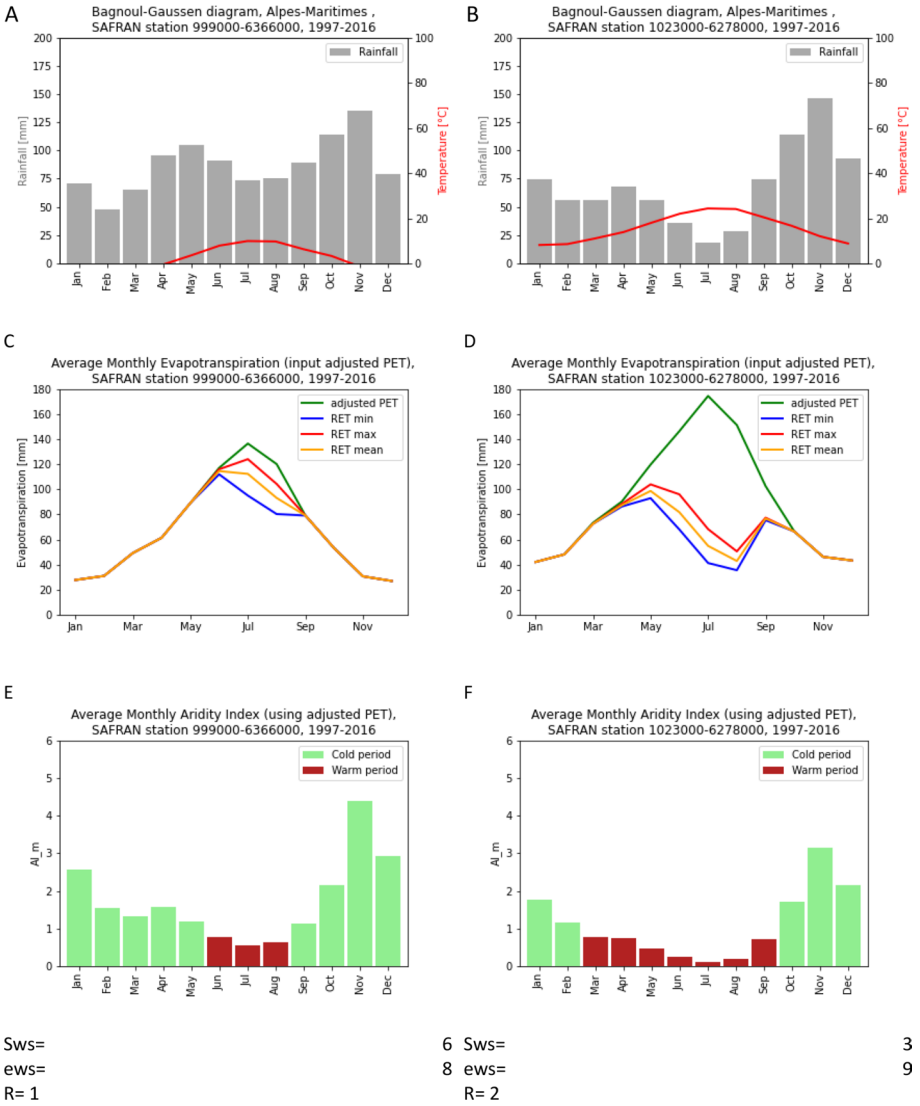

Sws= 6 Sws= 3
ews= 8 ews= 9
R= 1 R= 2

Fig. 7 Results of the climate analysis for a mountain station and a Mediterranean station: Bagnoul-Gaussen diagrams (Comparison of mean monthly rainfall and mean monthly temperature) (**A**, **B**), evapotranspiration diagrams (**C**, **D**) and aridity index charts (**E**, **F**). The range of monthly mean RET values obtained by varying RD and AWSC is represented in (C, D) by RET min and RET max, respectively the upper and lower bounds of the range of values. The mean value, RET mean, was selected as result. Ajusted PET on this same graph was obtained from the average of daily values from the rainfall dataset

Figure 8 displays for MPRC, 5% and 50% (best fit line) NEP thresholds superposed over a scatterplot of the conditions, and statistical distributions of δ (difference of the logarithm of the data points' cumulated rainfall and the best fit line,. In supplementary material section, detailed equation (A), and MRC (B), 5% and 50% NEP thresholds are provided.

Table 1 Characteristics (description of conditions, validity range, equation, and relative uncertainty) of the thresholds obtained from the calibration set. The coefficients of the most used 5% NEP thresholds are represented with a bold font. Equations of the 5% NEP thresholds obtained with constant climate-dependent parameters (R = 1 and R = 4) are included

Conditions	Equation	NEP	α	Δα	Δα/α
Climate-dependent R MRC 446 conditions Validity range D∈[3, 274] h	$E = (\alpha \pm \Delta\alpha)D^{0.27\pm0.04}$	50	24.47	4.15	0.17
		20	14.48	2.67	0.18
		10	11.02	2.13	0.19
		5	**8.79**	**1.77**	**0.20**
		1	5.75	1.25	0.22
Climate-dependent R MPRC 218 conditions Validity range D∈[3, 169] h	$E = (\alpha \pm \Delta\alpha)D^{0.31\pm0.04}$	50	22.66	3.52	0.16
		20	13.55	2.21	0.16
		10	10.35	1.76	0.17
		5	**8.29**	**1.46**	**0.18**
		1	5.47	1.04	0.19
R = 1, NEP = 5% 215 MPRC	$E = (5.8 \pm 1.3)D^{0.41\pm0.06}$				
R = 4, NEP = 5% 200 MPRC	$E = (16.0 \pm 3.6)D^{0.08\pm0.06}$				

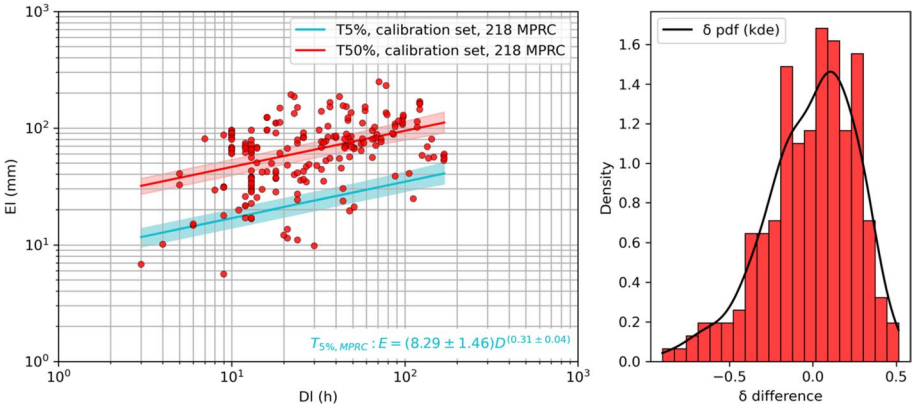

Fig. 8 T5% and T50% thresholds, superposed to scatterplots of conditions, and statistical distributions of δ along with probability density function estimated by Kernel Density Estimation MPRC. The size of the marker of the MRC scatterplot is related to the likeliness of the condition

The probability density functions of the δ variable estimated from the distributions by Kernel Density Estimation (kde) are as well represented on the graph. The size of a scatter point on the MRC graph represents the likeliness of the condition (larger points are MPRC). The MRC dataset contains twice as many conditions (446 conditions) as the MPRC dataset does (218 conditions).

37 (8%) and 219 (49%) conditions are respectively observed below the T5% and T50% datasets for the MRC dataset. For the MPRC dataset, we counted 15 (7%) and 102

(47%) conditions below thresholds of same NEP. The thresholds obtained with MRC have a wider validity range (3–274 h) than the MPRC thresholds (3–169 h).

The distributions of the conditions in the (D, E) space are further investigated by computing cumulative distribution functions. The validation sets are included in the statistics. The cumulative distribution functions (CDF) of the cumulated rainfall and duration of both MRC and MPRC of the calibration and validation set are plotted on Fig. 9. The graph plotting the distributions of the durations indicates that MRC of both calibration and validation sets tend to have longer durations than MPRC. A slight difference between calibration set and validation set is noted in the statistics of cumulated rainfall values. There is a higher number of values (steeper curve) around 100 mm in the calibration set than in the validation set. This difference is smaller for the MRC than for the MPRC.

4.3 Validation

The thresholds obtained from the calibration set, described above, are compared to all the rainfall sub-events generated from the validation set. Only 4 entities out of the initial 75 landslides of the validation set were discarded, once again because of the delay rainfall/landslide exceeding 48 h. The pre-processing of these sub-events, following the method developed by (Gariano et al. 2015), explained below, is done.

The scatter-plot of the different sub-events in the D,E space, along with the 1%, 5% and 10% NEP MPRC thresholds obtained from the validation set is available on Fig. 10. Statistics (mean, min, max, standard deviations and quartiles) describing the different categories of sub-events are available on Table 2.

We notice that the statistics are quite similar for triggering sub-events, and sub-events recorded at the time of the landslide by neighboring rain gauges. We also acknowledge the drastic difference in cumulated rainfall for the triggering and non-triggering sub-events.

After a deletion of 7917 sub-events, 75 triggering sub-events and 17,095 non-triggering sub-events are considered to compute scores. For each non-exceedance probability, we counted true positives (TP), false negatives (FN), false positives (FP) and true negatives (TN) by comparing the observed data of the validation period and the thresholds of the calibration set. From these numbers, we calculated skill scores: probability of detection (POD), probability of false detection (POFD), probability of false alarm (POFA) and Hanssen and Kuipers skill score (HK). The scores are displayed for some NEP in Table 3. All the NEP can be seen in Supplementary materials section.

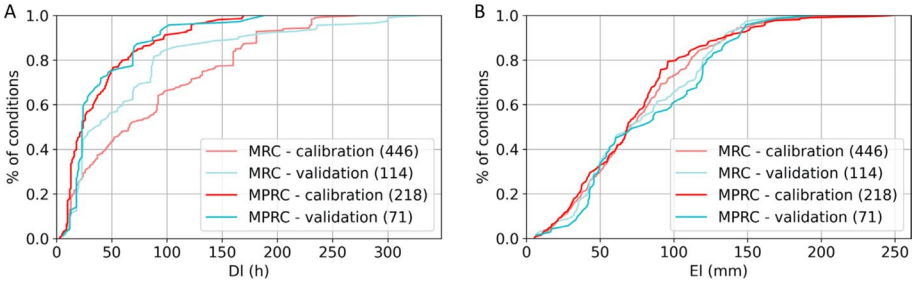

Fig. 9 Cumulative distribution functions (CDF) of the rainfall durations (**A**) and cumulated rainfalls (**B**) of the MRC and MPRC of calibration and validation datasets

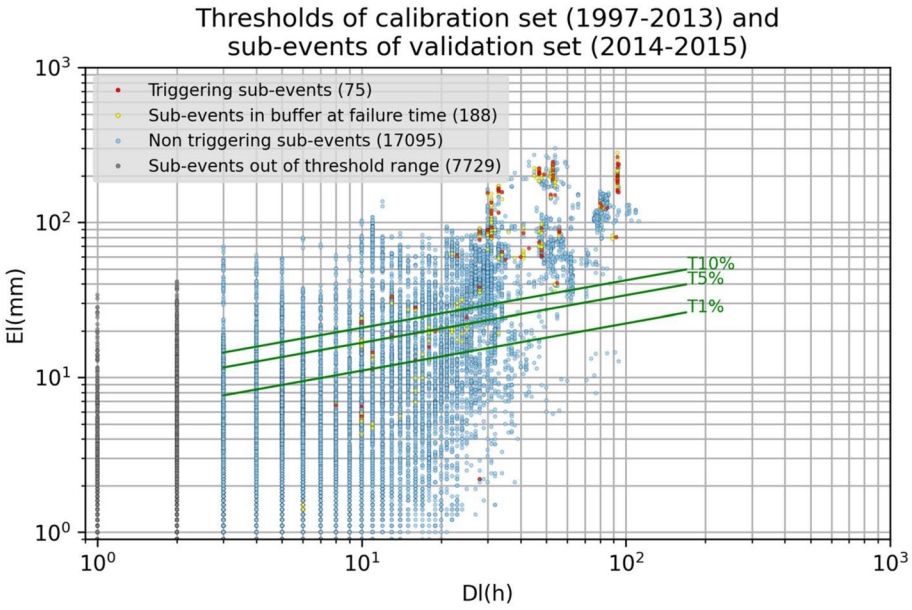

Fig. 10 Scatterplot of the validation sub-events and thresholds T10%, T5% and T1% obtained from the calibration set. Sub-events are color-coded. Red and blue markers respectively stand for triggering and non-triggering sub-events. Yellow markers, corresponding to triggering sub-events recorded by neighboring rain gauges, and grey markers exceeding the threshold bounds were discarded in the next steps

An optimal system can predict with confidence true positives as well as true negatives. The ROC analysis (Fawcett 2006), built on this assumption, compares binary classifiers based on their POFD and POD scores. In our case, MPRC thresholds generated with different non-exceedance probabilities are represented as a curve on a POFD/POD space (Fig. 11). The best prediction performance corresponds to a POD equal to 1 and a POFD equal to 0 (sensitivity and specificity equal to 1, red marker on Fig. 11). Conversely, the line POFD = POD ("no gain line") corresponds to a random classifier. δ, in Table 3, is the ROC space distance of the threshold to the best prediction performance.

T35% is identified as best performing threshold according to both the HK score and the δ coefficient obtained through the ROC curve.

5 Discussion

This study leads to the creation of statistical rainfall thresholds for landslide triggering for Alpes-Maritimes department, from high resolution rainfall data, considering different non-exceedance probabilities. A validation step enables the identification of best performing thresholds. These results pave the way towards a regional operational landslide monitoring system.

Table 2 Statistics (mean, standard deviation, min, max, quartiles) of the duration and cumulated rainfall of the sub-events identified over the validation period, grouped by categories

Sub-event category	Number of sub-events	Duration D [hours]							Cumulated rainfall E [mm]						
		Mean	Std	Min	25%	50%	75%	Max	Mean	Std	Min	25%	50%	75%	Max
Triggering	75	48	27	8	30	47	56	94	119	75	2	61	115	190	264
In buffer at failure time	188	43	25	3	25	41	53	94	108	76	1	35	88	185	281
Non triggering	17,095	14	15	3	5	9	17	112	17	29	0	2	7	19	301
Out of range	7729	1	1	1	1	1	2	2	2	3	0	0	1	1	41

Table 3 Confusion matrix (TP, FP, TN, FN) and skill scores (POD, POFD, POFA, HK, δ) obtained for thresholds at different NEPs; best results for each score are shown in bold. The optimal scores (perfect classifier) that would be obtained for this dataset are displayed in the last line

NEP	TP	FN	FP	TN	POD	POFD	POFA	HK	δ
50	51	24	**1261**	**15,834**	0.680	**0.074**	**0.961**	0.606	0.328
20	61	14	2657	14,438	0.813	0.155	0.978	0.658	0.243
10	64	11	3742	13,353	0.853	0.219	0.983	0.634	0.263
5	66	9	4637	12,458	0.880	0.271	0.986	0.609	0.297
1	70	5	6408	10,687	0.933	0.375	0.989	0.558	0.381
Optimal score	75	0	0	17,095	1	0	0	1	0

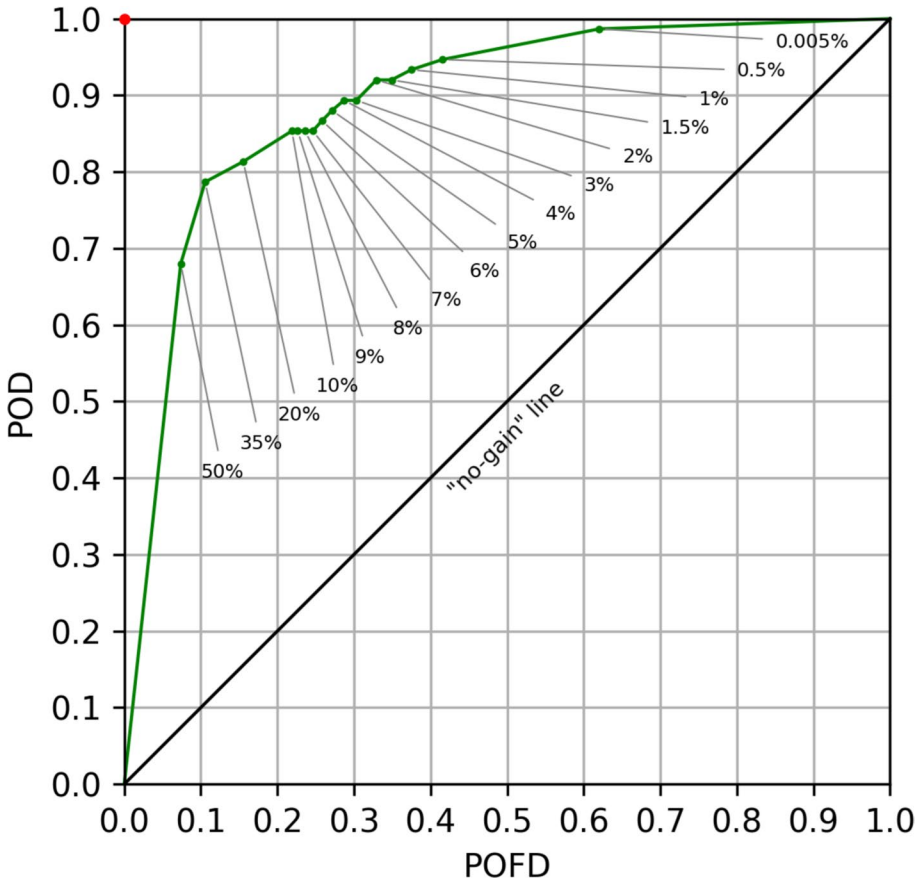

Fig. 11 ROC analysis curve. Each MPRC threshold is represented as a point in the POFD/POD space. The best performing threshold is the one closest (smaller δ) to the perfect classifier (red marker)

5.1 Climate analysis

The climate analysis yields longer warm seasons in the south of the department and along the coastline. This corroborates the climate zoning described by other studies, detailed in 10. The value of the ratio R, proportional to the length of the warm season, tends as well to be higher in the south. Computing rainfall events and sub-events separators separately for each grid point enables to assess the impact of rainfall locally, based on the climate. A rainfall normalization step is not compulsory when choosing this option.

The thresholds obtained for varying R ratios are plotted on Fig. 12 from the data of Table 1. They yield information on the sensitivity of the method to the climate-dependent parameters. We note significant differences in the threshold slopes. This can be explained by MPRC having a longer duration for similar accumulated rainfall for higher R ratios. Indeed, choosing a higher R ratio means considering longer event and sub-event separators during the cold season, and eventually designing longer events. The significant differences in the resulting thresholds stress the importance of these parameters in the threshold design.

5.2 Threshold calibration

First of all, the number of landslide triggering rainfall events is recommended to be superior to 200 to reduce sample variation when using a frequentist method based on landslide occurrence (Peres and Cancelliere 2021): both MRC and MPRC calibration sets fulfill this requirement. However, the relative uncertainty $\Delta\alpha/\alpha$ is recommended to be inferior to 0.10 in an operational landslide warning system (Peruccacci et al. 2012), yet we have obtained

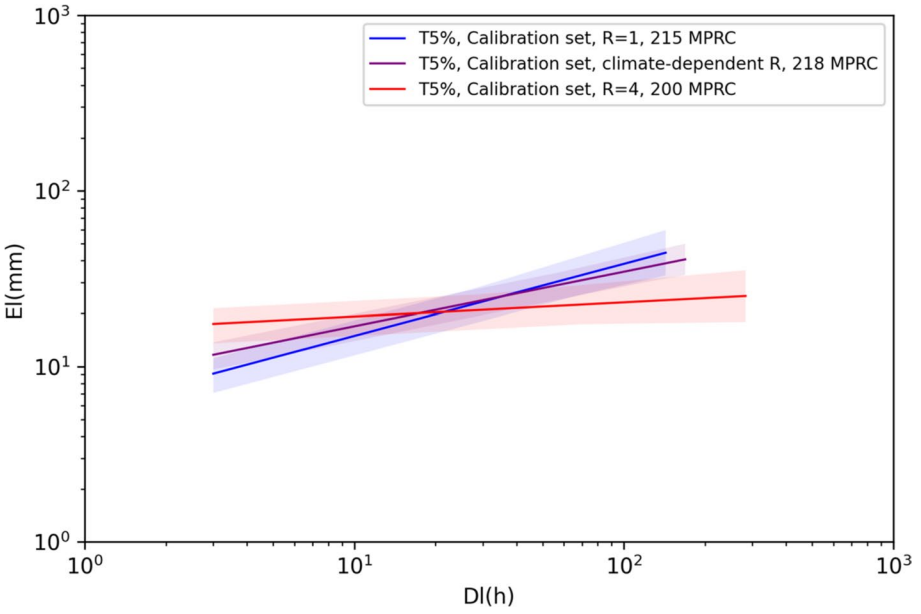

Fig. 12 Comparative plot of the 5% NEP thresholds obtained for the calibration set changing the climate-dependent R ratio (R computed separately for each station, R = 1 and R = 4)

in the best case (MPRC) relative uncertainties ranging from 0.16 to 0.23. Solutions to lower the relative uncertainty could either be to increase the number of landslides in the database, or to narrow the study zone around more homogeneous D, E conditions. Then, more than 15% of the landslide events of the calibration set (51 out of a total of 269 events) have been discarded due to the lack of immediate rainfall triggers. It is necessary to analyze what induced these landslides. Within the different hypotheses that might explain this, the contribution of the snowmelt, or even snowmelt events, might be significant (Krøgli et al. 2018; Mostbauer et al. 2018), especially in Köppen climates Dfb and ET. This phenomenon is not accounted for in this study, yet is to consider as a non-negligible part of Alpes-Maritimes is covered by the Alps (Mercantour range).

The thresholds obtained for the Alpes-Maritimes department were compared to thresholds issued from the literature computed as well with the CTRL-T algorithm, for Liguria (Melillo et al. 2018), Slovenia (Jordanova et al. 2020), for different climates in Italy found in the Maritime Alps (Peruccacci et al. 2017), and for the Italian Alps (Peruccacci et al. 2017; Palladino et al 2018).

These two neighboring regions feature climatic characteristics similar to our study zone: Alpes-Maritimes department encapsulates the Köppen climates Csa, Csb, Cfb and Dfb found both in Liguria (Csa, Csb, Cfb) and Slovenia (Cfb, Dfc, ET) (Rubel et al. 2017). Although we obtained best results for T35%, T5% were compared, being more commonly used. We used the Ligurian threshold obtained taking $R = 2$ and the Slovenian threshold describing zones of the country whose mean annual rainfall (MAR) ranges between 800 and 1300 mm, most alike Alpes-Maritimes. The comparative plot are available in Fig. 13.

In subplot A, we only compare thresholds made for climates in Italy that are found in the Maritime Alps. Csa designates the hot summer Mediterranean climate, encountered in

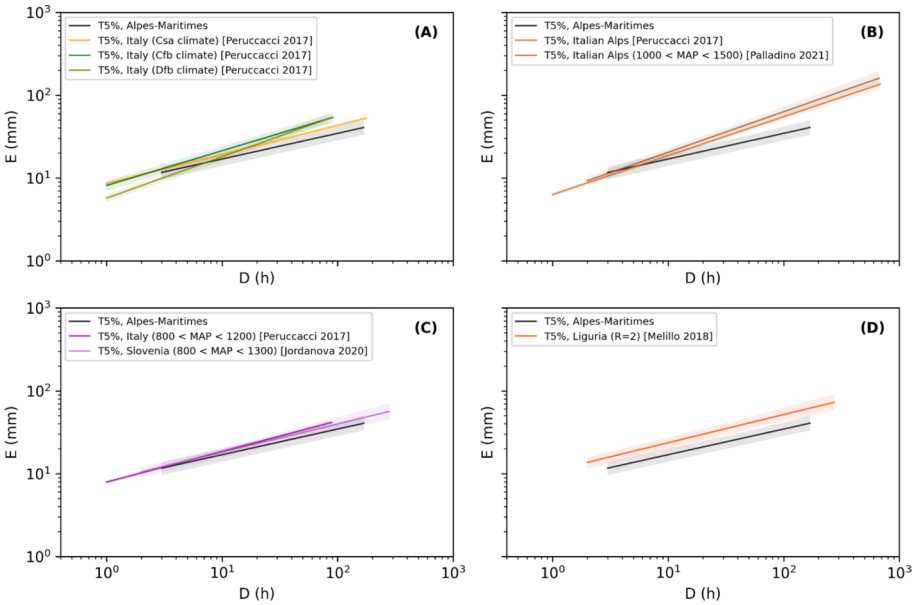

Fig. 13 Comparative plot of T5% ED thresholds obtained in different studies using CTRL-T for Alpes-Maritimes, Slovenia, Liguria, different climates in Italy found in the Maritime Alps, and for the Italian Alps (Melillo et al. 2018; Peruccacci et al. 2017; Palladino et al 2018; Jordanova et al. 2020)

Coastal Alpes-Maritimes. Dfb describes a cool continental climate, as found in the mountainous area of the department. Finally, Cfb describes the transition sector between these two zones. The threshold is closer to the Csa Mediterranean climate. As this climate is characterized by short and intense rainfall events in the autumn (Météo-France 2024), the slope of the threshold is less important than for the other climates. We explain the similitude to our threshold by the fact that the landslide inventory is concentrated on the coastal part of the department. In subplot B, the thresholds established for the Italian Alps are very different from the one obtained in the Alpes Maritime department, which corroborates the point made above. in subplot C, we compare our threshold with thresholds based on average annual precipitation criteria. They are close, which means that mean annual rainfall could be a decisive criterion for defining thresholds. Finally in subplot D the rainfall thresholds have similar slopes. The intercept of the threshold obtained by (Melillo et al. 2018) is higher, which physically translates to more intense triggering conditions in Liguria. We expected our results to be most like Ligurian thresholds given the climatic and geographical proximity, yet this was not the case.

More general comments can be made regarding the hypothesis inherent to the frequentist method. The threshold equation coefficients are obtained from a Gaussian curve modeled over the probability distribution function of the δ variable, derived from the distribution with Kernel Density Estimation. However, we obtained in this work negatively skewed probability density functions, and even bimodal characteristics for MRC. This might explain why for MRC and MPRC, 7% and 8% of conditions were observed below the T5% instead of the expected 5%. This weakness must not be ignored before operational use as it leads to underestimating triggering conditions.

5.3 Validation

From the validation results, we remark that some sub-events with a duration inferior to the thresholds' lower boundary (3 h) have very high associated cumulated rainfall. Given the lack of calibration MPRC with such durations, we are not able to make predictions for these sub-events, yet they definitely could trigger landslides given their intensities.

The scores reveal that our thresholds are efficient when it comes to identify a triggering event or a non-triggering event (high POD, low POFD). For our optimal T35% threshold we obtained a POD of 0.79, which corresponds to identifying the occurrence of 4 landslides out of 5. However the method yields mediocre results when it comes to avoiding false alarms: the lowest POFA we obtain is equal to 0.961 – only one out of twenty forecast events actually occurs. This is explained by the scarcity of landslide data, compared to non-triggering rainfall information.

This is problematic when it comes to the implementation of a warning system, as a high number of false alarms lead to a loss of credibility and acceptance of the system. On the other hand, a low number of missed alarms is compulsory for a strong EWS as the security of people is the fundamental target of the EWS. In that way a compromise has to be done, and an optimal threshold should be defined based on the expected objectives of the EWS.

Both the Hanssen-Kuipers skill score and the delta metric indicate that the threshold with a 35% NEP design is the most reliable. Other studies (Gariano et al. 2015; Jordanova et al. 2020), using as well the ROC curve methodology obtained thresholds with lower NEPs (7–15%) as best results. We can explain our different results by the non-Gaussian distribution of the delta variable: the number of conditions below the T35% threshold is overestimated – it is equivalent to lower NEP thresholds.

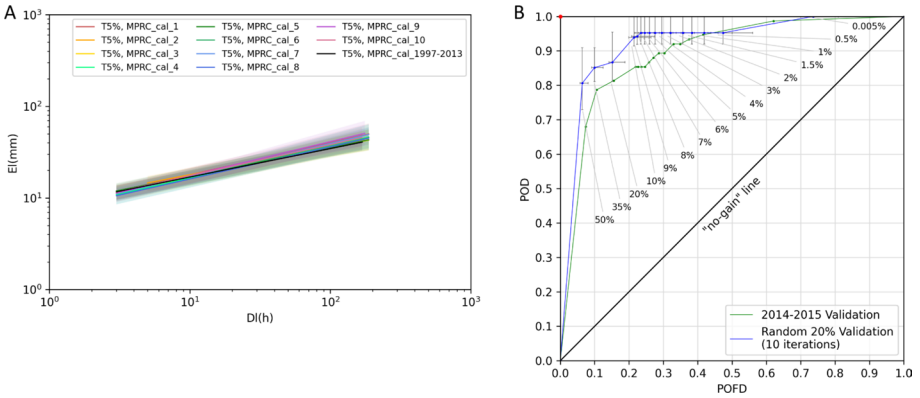

Fig. 14 **a** 5% NEP MPRC Thresholds obtained taking 1997–2013 as calibration period (black) versus randomly selecting 80% of landslides for calibration (10 iterations, colors); **b** ROC curves obtained taking 2014–2015 as validation period (green) versus randomly selecting 20% of landslides for validation (10 iterations, blue). The error bars represent the minimal and maximal score obtained for each NEP

Another limitation to our approach is that we work with rainfall sub-events for the validation, whereas the thresholds were obtained from conditions (combinations of rainfall sub-events). This explains why, for the validation set, we have more triggering sub-events (75) than MPRC (71). It is not possible to compute conditions for the validation period, given that a landslide date is required in the process. The consequences are that some of the sub-events used in the validation process are not representative of the triggering condition, especially knowing that percolation is only taken into account when computing conditions.

The analysis of the distribution of all conditions shows that conditions from the validation set have higher cumulated rainfall than those from the calibration set. This implies that the validation set is not fully representative of the regional rainfall regime; as seen in Fig. 2 and Fig. 4, the validation set is not representative of mountainous climate, as landslides are more located within Mediterranean climate. Repeating the validation process over different time ranges would solve this issue.

To investigate further this issue and characterize the resulting bias, we compared thresholds obtained in this study to those resulting from 10 random subdivisions of landslides (80% calibration, 20% validation). The following results were obtained in Fig. 14:

All thresholds and their uncertainty ranges overlap: this suggests that for our dataset, a pool of conditions based on 80% of landslides are sufficient to obtain robust thresholds with this method, and no bias arises from the definition of the calibration set. However, the scores obtained using 2014–2015 as the validation period are lower for the higher NEP than those obtained by randomly selecting 20% of landslides for validation. The choice of the two years for the validation period introduces a bias in the validation scores. Overall, the definition of the calibration and validation years does not lead to a biased threshold as the method is robust enough, although the validation scores are lower.

5.4 General remarks

More broad comments can be made regarding the methodological approach. The novel use of high-resolution rainfall data and evapotranspiration data is a strength of this

work, although the method could use other improvements. Among them, the incorporation of other factors than rainfall duration and cumulated rainfall, such as antecedent rainfall and snowmelt, would represent a step forward.

The use of gridded rainfall data of high spatial (1 km) and temporal (hourly) resolution is an asset of this study. Rainfall triggering conditions are reconstructed with a high accuracy, which is especially relevant given the complex orographic system of Alpes-Maritimes and the rainfall typology of the Mediterranean climate (Segoni et al. 2018). With an important relief, meteorological conditions vary significantly over short distances. Therefore, capturing rainfall conditions within a very small radius of the landslide is a major asset of this work.

Also, the use of coarse temporal resolution rainfall data drastically increases uncertainties (Gariano et al. 2020). However, the bias induced by the clustering of landslides along the coastline persists- we must ponder that the thresholds account more for the Mediterranean zone than the Mountain zone of the region.

The addition of Safran data to compute sws, ews and R parameters improves the description of the heterogeneous regional climate. As replacing evapotranspiration approximations by data enhance the results of the climate analysis, the next improvement steps would be to do the same with the approached soil and vegetation characteristics considering the existence and availability of such data. More generally, the effective rainfall constitutes a key issue, with considering in particular the infiltrated water.

Then, a weakness of our approach is that Safran mesh points were selected using only a criterion of geographical distance, even though it is known that local climatic conditions severely change with altitude. This criticism can be spread to the method of selection of rain gauges from landslide coordinates in the code CTRL-T.

Next, the high uncertainty of the thresholds was raised in a previous section. Even though solutions were pointed out to reduce this uncertainty, the main weakness resides in the small number of landslide events in our inventory. Moreover, as analysed by (Peres et al. 2018), the time uncertainty on the landslide initiation may have some impacts on rainfall threshold. Several studies (Leonarduzzi and Molnar 2020; Hirschberg et al. 2021) have pointed out the frequentist method for neglecting non triggering rainfall information, crucial for the assessment of the false alarm rate. The second study even adds a threshold adjustment step from the obtained TSS score, which integrate the information of the non-triggering events. Moreover, studies have shown that thresholds obtained from a frequentist method focused on triggering rainfall lack robustness, and that frequentist methods centered on non-triggering or triggering and non-triggering events lead to thresholds with a higher sensitivity and specificity (Peres and Cancelliere 2021).

Apart from the neglect of non-triggering rainfall data, another limitation of this method is that it considers only duration and cumulated rainfall as landslide trigger estimators, whereas it is commonly known that the process is complex and multivariate. New research approaches include improving thresholds obtained by a frequentist method by machine learning techniques, integrating significant variables such as rainfall peak intensity (Distefano et al. 2021). We can imagine incorporating the information of the rainfall antecedent, and the snowmelt, another significant indicators, in the same fashion. Moreover, Another main drawback of landslide rainfall-based Te-EWS is their poor spatial prediction capacity: a threshold overcoming produces an alert for the entire area encompassing the events used for calibration, while the location of expected landslides is poorly constrained. This is related to the multifactorial character of landslide triggering, which is not only controlled by meteorological forcing, but also by local conditions. To improve the spatial prediction of EWS, some authors proposed to combine rainfall fields to susceptibility maps based on

predisposition factors, such as relief, geology, land-use and landforms (Tiranti et al. 2014; Berenguer et al. 2015).

6 Conclusion

Rainfall thresholds are models that aim to specify rainfall conditions able to trigger landslides. When issued from empirical data, they can be defined at a regional scale and therefore can be integrated to Landslide Early Warning Systems (LEWS).

In this work, we have computed statistical cumulated rainfall/duration rainfall thresholds for the Alpes-Maritimes French department, a mountain region subjected to intense Mediterranean type rainfall. The CTRL-T algorithm (Melillo et al. 2018) was used to generate the thresholds, as we favored automatic and objective approaches based only on rainfall data, a landslide inventory and regional climatic characteristics.

Our landslide inventory was split in two parts: thresholds were first computed from a calibration subset, and then tested with an independent validation subset. We obtained thresholds, for different non-exceedance probabilities (design percentage of false negatives), and for two distinct pools of conditions: Multiple Rainfall Conditions, and Most Probable Rainfall Conditions, restraining the number of conditions to one for each landslide. The best performing thresholds is the T35% MPRC threshold. This work represents novel scientific progress by (a) making a case study of empirical rainfall thresholds for Alpes-Maritimes, (b) using high-resolution rainfall data and (c) adapting the method to climatically heterogeneous zones.

However, some weaknesses of this work can be underlined: the uncertainty, linked to the number of events in the landslide inventory, seems too high for a direct operational use. Next steps for further improvement include integrating other factors, such as non-triggering rainfall information, and rainfall antecedent.

Supplementary Information The online version contains supplementary material available at https://doi.org/10.1007/s11069-024-06941-2.

Acknowledgements The authors would like to thank the French meteorological service Météo-France for providing the climate datasets, and J. Rohmer for his valuable advice regarding the design of the validation scheme.

Funding This work is financed by the French National Research Agency (ANR) through ANR VIGIMONT project (VIGIlance MONTagne – Mountain Vigilance : Forecasting the risk of landslides and debris flows in mountainous areas). ANR-22-CE04-0021. It is also financially supported by a Bureau de Recherches Géologiques et Minières (BRGM) research project, and by the French Ministry of the Ecological Transition (MTE).

Declarations

Conflict of interest The authors declare no competing interests.

References

Abraham MT, Satyam N, Rosi A et al (2021) Usage of antecedent soil moisture for improving the performance of rainfall thresholds for landslide early warning. CATENA 200:105147. https://doi.org/10.1016/j.catena.2021.105147

Aleotti P (2004) A warning system for rainfall-induced shallow failures. Eng Geol 73:247–265. https://doi.org/10.1016/j.enggeo.2004.01.007

Alvioli M, Baum RL (2016) Parallelization of the TRIGRS model for rainfall-induced landslides using the message passing interface. Environ Model Softw 81:122–135. https://doi.org/10.1016/j.envsoft.2016.04.002

Berenguer M, Sempere-Torres D, Hürlimann M (2015) Debris-flow forecasting at regional scale by combining susceptibility mapping and radar rainfall. Nat Hazards Earth Syst Sci 15:587–602. https://doi.org/10.5194/nhess-15-587-2015

Brunetti MT, Peruccacci S, Rossi M et al (2010) Rainfall thresholds for the possible occurrence of landslides in Italy. Nat Hazards Earth Syst Sci 10:447–458. https://doi.org/10.5194/nhess-10-447-2010

Caine N (1980) The rainfall intensity: duration control of shallow landslides and debris flows. Geogr Ann Ser Phys Geogr 62:23–27. https://doi.org/10.2307/520449

Distefano P, Peres DJ, Scandura P, Cancelliere A (2021) Brief communication: Rainfall thresholds based on Artificial neural networks can improve landslide early warning. Nat Hazards Earth Syst Sci [preprint] https://doi.org/10.5194/nhess-2021-206

Durand Y, Brun E, Merindol L et al (1993) A meteorological estimation of relevant parameters for snow models. Ann Glaciol 18:65–71. https://doi.org/10.3189/S0260305500011277

Fawcett T (2006) An introduction to ROC analysis. Pattern Recognit Lett 27:861–874. https://doi.org/10.1016/j.patrec.2005.10.010

Gariano SL, Brunetti MT, Iovine G et al (2015) Calibration and validation of rainfall thresholds for shallow landslide forecasting in Sicily, Southern Italy. Geomorphology 228:653–665. https://doi.org/10.1016/j.geomorph.2014.10.019

Gariano SL, Sarkar R, Dikshit A et al (2019) Automatic calculation of rainfall thresholds for landslide occurrence in Chukha Dzongkhag, Bhutan. Bull Eng Geol Environ 78:4325–4332. https://doi.org/10.1007/s10064-018-1415-2

Gariano SL, Melillo M, Peruccacci S, Brunetti MT (2020) How much does the rainfall temporal resolution affect rainfall thresholds for landslide triggering? Nat Hazards 100:655–670. https://doi.org/10.1007/s11069-019-03830-x

Guzzetti F, Peruccacci S, Rossi M, Stark CP (2007) Rainfall thresholds for the initiation of landslides in central and southern Europe. Meteorol Atmospheric Phys 98:239–267. https://doi.org/10.1007/s00703-007-0262-7

Guzzetti F, Peruccacci S, Rossi M, Stark CP (2008) The rainfall intensity–duration control of shallow landslides and debris flows: an update. Landslides 5:3–17. https://doi.org/10.1007/s10346-007-0112-1

Hirschberg J, Badoux A, McArdell BW et al (2021) Limitations of rainfall thresholds for debris-flow prediction in an Alpine catchment. Nat Hazards Earth Syst Sci. https://doi.org/10.5194/nhess-2021-135

Joly D, Brossard T, Cardot H et al (2010) Les types de climats en France, une construction spatiale. Cybergeo. https://doi.org/10.4000/cybergeo.23155

Jordanova G, Gariano SL, Melillo M et al (2020) Determination of empirical rainfall thresholds for shallow landslides in slovenia using an automatic tool. Water 12:1449. https://doi.org/10.3390/w12051449

Kottek M, Grieser J, Beck C et al (2006) World map of the Köppen-Geiger climate classification updated. Meteorol Z 15:259–263. https://doi.org/10.1127/0941-2948/2006/0130

Krøgli IK, Devoli G, Colleuille H et al (2018) The Norwegian forecasting and warning service for rainfall- and snowmelt-induced landslides. Nat Hazards Earth Syst Sci 18:1427–1450. https://doi.org/10.5194/nhess-18-1427-2018

Leonarduzzi E, Molnar P (2020) Deriving rainfall thresholds for landsliding at the regional scale: daily and hourly resolutions, normalisation, and antecedent rainfall. Nat Hazards Earth Syst Sci 20:2905–2919. https://doi.org/10.5194/nhess-20-2905-2020

Marra F, Nikolopoulos EI, Creutin JD, Borga M (2014) Radar rainfall estimation for the identification of debris-flow occurrence thresholds. J Hydrol 519:1607–1619. https://doi.org/10.1016/j.jhydrol.2014.09.039

Melillo M, Brunetti MT, Peruccacci S et al (2015) An algorithm for the objective reconstruction of rainfall events responsible for landslides. Landslides 12:311–320. https://doi.org/10.1007/s10346-014-0471-3

Melillo M, Brunetti MT, Peruccacci S et al (2018) A tool for the automatic calculation of rainfall thresholds for landslide occurrence. Environ Model Softw 105:230–243. https://doi.org/10.1016/j.envsoft.2018.03.024

Météo-France (2023) Événements mémorables - Pluies extrêmes en France métropolitaine. http://pluiesextremes.meteo.fr/france-metropole/-Evenements-memorables-.html. (Last Access 23 June 2023)

Météo-France (2024) Un peu de géographie – Pluies extrêmes en France métropolitaine. http://pluiesextremes.meteo.fr/france-metropole/Un-peu-de-geographie.html. Accessed on 24 July 2024

Mostbauer K, Kaitna R, Prenner D, Hrachowitz M (2018) The temporally varying roles of rainfall, snowmelt and soil moisture for debris flow initiation in a snow-dominated system. Hydrol Earth Syst Sci 22:3493–3513. https://doi.org/10.5194/hess-22-3493-2018

ORRM (2023) Observatoire Régional des Risques Majeurs en Provence-Alpes-Côte d'Azur. http://observatoire-regional-risques-paca.fr/. (Last Access 23 June 2023)

Palladino MR, Viero A, Turconi L, Brunetti MT, Peruccacci S, Melillo M, Luino F, Deganutti AM, Guzzetti F (2018) Rainfall thresholds for the activation of shallow landslides in the Italian Alps: the role of environmental conditioning factors. Geomorphology 303:53–67. https://doi.org/10.1016/j.geomorph.2017.11.009

Peres DJ, Cancelliere A (2021) Comparing methods for determining landslide early warning thresholds: potential use of non-triggering rainfall for locations with scarce landslide data availability. Landslides 18:3135–3147. https://doi.org/10.1007/s10346-021-01704-7

Peres DJ, Cancelliere A, Greco R, Bogaard TA (2018) Influence of uncertain identification of triggering rainfall on the assessment of landslide early warning thresholds. Nat Hazards Earth Syst Sci 18:633–646. https://doi.org/10.5194/nhess-18-633-2018

Peruccacci S, Brunetti MT, Luciani S et al (2012) Lithological and seasonal control on rainfall thresholds for the possible initiation of landslides in central Italy. Geomorphology 139–140:79–90. https://doi.org/10.1016/j.geomorph.2011.10.005

Peruccacci S, Brunetti MT, Gariano SL, Melillo M, Rossi M, Guzzetti F (2017) Rainfall thresholds for possible landslide occurrence in Italy. Geomorphology 290:39–57. https://doi.org/10.1016/j.geomorph.2017.03.031

Piciullo L, Tiranti D, Pecoraro G et al (2020) Standards for the performance assessment of territorial landslide early warning systems. Landslides 17:2533–2546. https://doi.org/10.1007/s10346-020-01486-4

Quintana-Seguí P, Le Moigne P, Durand Y et al (2008) Analysis of near-surface atmospheric variables: validation of the SAFRAN analysis over France. J Appl Meteorol Climatol 47:92–107. https://doi.org/10.1175/2007JAMC1636.1

Rubel F, Brugger K, Haslinger K, Auer I (2017) The climate of the European Alps: Shift of very high resolution Köppen-Geiger climate zones 1800–2100. Meteorol Z 26:115–125. https://doi.org/10.1127/metz/2016/0816

Segoni S, Rossi G, Rosi A, Catani F (2014) Landslides triggered by rainfall: a semi-automated procedure to define consistent intensity–duration thresholds. Comput Geosci 63:123–131. https://doi.org/10.1016/j.cageo.2013.10.009

Segoni S, Lagomarsino D, Fanti R et al (2015) Integration of rainfall thresholds and susceptibility maps in the Emilia Romagna (Italy) regional-scale landslide warning system. Landslides 12:773–785. https://doi.org/10.1007/s10346-014-0502-0

Segoni S, Piciullo L, Gariano SL (2018) A review of the recent literature on rainfall thresholds for landslide occurrence. Landslides 15:1483–1501. https://doi.org/10.1007/s10346-018-0966-4

Staley DM, Kean JW, Cannon SH et al (2013) Objective definition of rainfall intensity–duration thresholds for the initiation of post-fire debris flows in southern California. Landslides. https://doi.org/10.1007/s10346-012-0341-9

Tabary P, Dupuy P, L'Henaff G et al (2012) A 10-year (1997–2006) reanalysis of quantitative precipitation estimation over France: methodology and first results. IAHS-AISH Publ 351:255–260

Teja TS, Dikshit A, Satyam N (2019) Determination of rainfall thresholds for landslide prediction using an algorithm-based approach: case study in the Darjeeling Himalayas. India Geosciences 9:302. https://doi.org/10.3390/geosciences9070302

Thornthwaite CW, Mather JR (1957) Instructions and tables for computing potential evapotranspiration and the water balance. Publications in Climatology X Number 3. Drexel Institute of Technology, Laboratory of Climatology, Centerton, New Jersey

Tiranti D, Rabuffetti D (2010) Estimation of rainfall thresholds triggering shallow landslides for an operational warning system implementation. Landslides 7:471–481. https://doi.org/10.1007/s10346-010-0198-8

Tiranti D, Cremonini R, Marco F et al (2014) The DEFENSE (debris Flows triggEred by storms – nowcasting system): an early warning system for torrential processes by radar storm tracking using a geographic information system (GIS). Comput Geosci 70:96–109. https://doi.org/10.1016/j.cageo.2014.05.004

Vidal J-P, Martin E, Franchisteguy L et al (2010) A 50-year high-resolution atmospheric reanalysis over France with the Safran system. Int J Climatol 30:1627–1644. https://doi.org/10.1002/joc.2003

Wilks D (2006) Statistical methods in the atmospheric sciences, 2nd edn. Academic Press, Elsevier